Encoding many channels on the same frequency through radio vorticity: first experimental test

Encoding many channels on the same frequency through radio vorticity: first experimental test

Fabrizio Tamburini[1,2,8]**, Elettra Mari**[3]**, Anna Sponselli**[1]**,
Bo Thidé**[4,5]**, Antonio Bianchini**[1] **and Filippo Romanato**[6,7]

[1] Department of Physics and Astronomy, University of Padova, vicolo dell'Osservatorio 3, I-35122 Padova, Italy
[2] CIVEN, Via delle Industrie 5, Torre Hammon I-30175, Venezia-Marghera, Italy
[3] CISAS, University of Padova, via Venezia 15, I-35131 Padova, Italy
[4] Swedish Institute of Space Physics, Box 537, Ångström Laboratory, SE-75121 Uppsala, Sweden
[5] Scuola Galileiana di Studi Superiori, University of Padova, via VIII Febbraio 1848, I-35122 Padova, Italy
[6] Department of Physics and Astronomy, University of Padova, via Marzolo 8 I-35100 Padova, Italy
[7] LaNN, Laboratory for Nanofabrication of Nanodevices, Venetonanotech, via Stati Uniti 4, I-35100 Padova, Italy
E-mail: fabrizio.tamburini@unipd.it

Abstract. We have shown experimentally, in a real-world setting, that it is possible to use two beams of incoherent radio waves, transmitted on the same frequency but encoded in two different orbital angular momentum states, to simultaneously transmit two independent radio channels. This novel radio technique allows the implementation of, in principle, an infinite number of channels in a given, fixed bandwidth, even without using polarization, multiport or dense coding techniques. This paves the way for innovative techniques in radio science and entirely new paradigms in radio communication protocols that might offer a solution to the problem of radio-band congestion.

S Online supplementary data available from stacks.iop.org/NJP/14/033001/mmedia

[8] Author to whom any correspondence should be addressed.

IOP Institute of Physics   Φ DEUTSCHE PHYSIKALISCHE GESELLSCHAFT

Contents

1. Introduction

The first radio signal transmitted and received by Guglielmo Marconi on 8 December 1895 started the wireless communication revolution [1]. Now information is mostly exchanged through wireless channels and the rapid increase of the use of mobile devices has led to congestion in the available radio bands even after the application of dense coding and channel sharing techniques [2]. Therefore, it is important to try to develop new methods that make it possible to utilize the electromagnetic (EM) spectrum better.

One way is to exploit fundamental physical properties of the EM field that hitherto have not been utilized in radio communications. To this end, we recall that the EM field can carry both energy and momentum. Whereas the Poynting vector $\mathbf{S}$ and the concomitant linear momentum $\mathbf{p} = \int \mathrm{d}^3 x \, \mathbf{S}$ (rational units) are associated with force action and therefore with translational dynamics, the angular momentum $\mathbf{J} = \int \mathrm{d}^3 x \, (\mathbf{x} \times \mathbf{S})$ is a conserved physical observable (constant of motion) that is associated with torque action and thus with rotational dynamics [3]. In a beam geometry as used in radio communications, the total angular momentum can be conveniently expressed as the sum of two components: $\mathbf{J} = \mathbf{\Sigma} + \mathbf{L}$. The component $\mathbf{\Sigma}$ represents the spin angular momentum (SAM), related to the polarization of the individual EM waves of the beam and thus with photon helicity. The component $\mathbf{L}$ represents the lesser-known orbital angular momentum (OAM) associated with the helicoidal phase profile of the EM beam in the direction orthogonal to the propagation axis. In a quantum picture $\mathbf{L}$ can be described as a superposition of discrete photon quantum eigenstates, each with a well-defined OAM value $\ell\hbar$, $\ell = 0, \pm 1, \pm 2, \ldots$ [4–7]. Hence, not only in mechanics but also in electromagnetism, OAM is a fundamental physical quantity that spans an infinite state space [8]. It offers, in addition to the conventional translational linear momentum and polarization (SAM) rotational degrees of freedom, which spans only a two-dimensional (2D) state space, additional rotational degrees of freedom that are distinctly different from SAM. Without increasing the frequency bandwidth, the OAM states can be used as a new, very large set of communication channels that are mutually orthogonal to each other in the OAM state space.

Here we report the results of real-world, outdoor radio experiments in the 2.4 GHz WiFi band that demonstrate the feasibility of increasing the wireless information transfer capacity over large distances by exploiting the OAM states [8] of EM waves. Our findings extend previous indoor laboratory test experiments in which the transmission of optical OAM states of

coherent laser [9] and radio [10] beams was demonstrated. The results reported here show that OAM and vorticity are preserved throughout the long-distance propagation over long distances and can indeed be utilized in radio communication.

Unlike already existing radio communication protocols that use the spatial phase distribution generated by a set of antennae to artificially increase the transmission bandwidth, the immediate advantage provided by a protocol based on the *physical* OAM states as independent communication channels is that of using the peculiar spatial phase distribution of each of these states as a reference pattern to generate, modulate and detect them in a better way.

OAM has found practical applications in many other fields such as radar [11], nanotechnology [12], quantum experiments [13] and also astronomy and space sciences [14–18], improving the resolving power of diffraction-limited optical instruments [19] and facilitating the detection of extrasolar planets [20] and Kerr black holes [21].

## 2. Transmitting with radio vortices

To date, there has been no report on the transmission of twisted radio beams in a real-world experiment. The results from our outdoor radio vorticity experiments demonstrate that when using a given radio frequency bandwidth around a fixed carrier frequency, the inherent orthogonality (in a Hilbert sense) of the denumerably infinite OAM state space can ideally provide, without increasing the frequency bandwidth, an arbitrarily large set of independent OAM transmission channels, each characterized only by its peculiar topological property. This new technique can be described as *topological diversity*.

In our radio vorticity communication experiments, we generated and detected two orthogonal OAM channels within a given fixed frequency band: one untwisted with OAM $\ell = 0$ and the other with an $\ell = 1$ OAM twist. Two identical WiFi FM transmitters, each with an output power of 2 W and driven by a signal generator, were tuned to the carrier frequency of 2.414 GHz to feed two antennae. In an FM transmission the amplitude and intensity of the EM wave remain constant in time; only the carrier frequency is modulated. The signal-to-noise ratio of the WiFi modules was 38 dB for the video channel and 45 dB for the audio band. The receiver sensitivity was -90 dBm, i.e. 10^{-9} mW. The transmitted signal bandwidths of both signals were 15 or 27 MHz, like those used in video signals.

The $\ell = 0$ source was radiated with linear polarization by a commercial 16.5 dBi gain Yagi–Uda antenna [22]. To generate the $\ell = 1$ vortex beam, we mechanically modified a 26 dBi commercial off-axis parabolic antenna, with diameter $D = 80$ cm, to attain an off-axis spiral parabolic-shaped phase mask reflector. The expected beam waist, given by the diffraction limit of the antenna, is $\delta\varphi = 1.22\lambda/D \approx 10.9°$, where λ is the radio wavelength. The half-power beam width (HPBW), i.e. the angular separation between the points on the antenna radiation pattern at which the power or, equivalently, the linear momentum, drops to half its maximum value is $\theta = k\lambda/D = 8.75°$. The characteristic parameter of the antenna, k, is a factor that depends on the shape of the reflector and the method of illumination. This $\ell = 1$ beam was also linearly polarized. Additional technical details of the experiment can be found in the appendix.

3. Intensity mapping of the field

As a first step, we characterized experimentally the physical properties of the twisted uncorrelated achromatic EM wave train, proving that vorticity and OAM can indeed be radiated
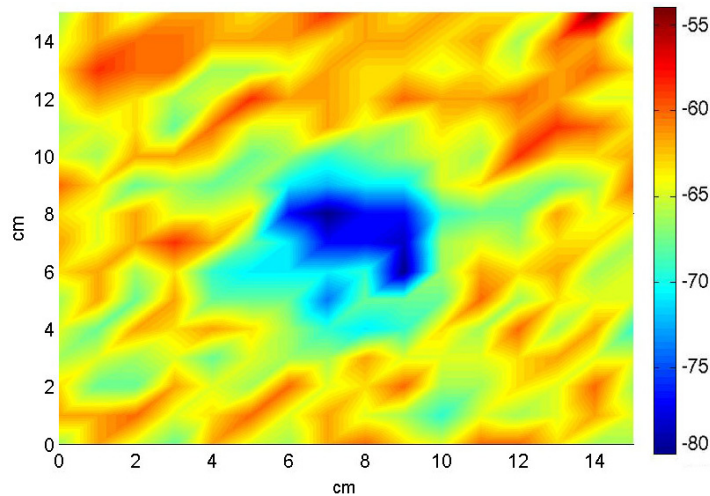
Figure 1. Intensity map of the radio beam vortex at $40\,\mathrm{m}$ ($\sim\!320\,\lambda$) in free space in the region around the singularity. The intensity distribution in this region exhibits fluctuations caused by perturbation and interference effects. The central dip indicates the region where the field singularity is located, less than $3\,\mathrm{cm}$ wide, with a measured intensity of $-82\,\mathrm{dBm}$. The actual position of the singularity was confirmed by the phase change measured by the two-antenna interferometer (see text). The scale is in centimetres.

into the far zone, in principle all the way to infinity [3]. In this way, we also proved that the topological properties of the twisted waves, namely the presence of the intensity (linear momentum) singularity and the spatial phase signature, are preserved in the far zone.

The intensity distribution of the radio vortex was mapped out $40\,\mathrm{m}$ (320λ) distant from the transmitting antenna. The HPBW diameter of the twisted parabolic antenna at $40\,\mathrm{m}$ distance is of the order of $6\,\mathrm{m}$. The radio noise background measured in a $15\,\mathrm{MHz}$ bandwidth centred on the carrier frequency $\nu = 2.414\,\mathrm{GHz}$ was $-90\,\mathrm{dBm}$. The polarization of the signal was linear and kept fixed horizontally. For safety reasons a calibrated $10\,\mathrm{dB}$ signal attenuator was inserted at the output of the transmission line.

As shown in figure 1, the region where the radio signal intensity, i.e. the received linear momentum, was undetectable had a diameter of $21\,\mathrm{cm}$ ($\sim\!1.7\lambda$) and we determined the position of the field singularity with an inaccuracy of $3\,\mathrm{cm}$ ($\sim\!0.24\lambda$). The experimental limitations were dictated by the resolving power of the spectrum analyser used for sampling the electric field. The average intensity measured in the $3\,\mathrm{cm}$ region around the singularity was $-82\,\mathrm{dBm}$.

That the minimum found was the phase singularity of the field was confirmed by measuring the phase distribution around it with a phase interferometer constructed from two identical Yagi–Uda antennae deployed along a baseline perpendicular to the direction of the transmitters. First we positioned the centre of the interferometer's baseline where the minimum of the field was measured and then we mechanically tilted the transmitting antenna in the horizontal and vertical directions and measured the ensuing phase change. Finally, we verified the phase and field intensity distribution of the Yagi–Uda antenna used for transmitting the untwisted signal. No appreciable phase twist in the Yagi–Uda beam was detected.

4. Radio transmission with orbital angular momentum

The purpose of the second stage of the experiment was to transmit, using the same set of antennae, on the same frequency of 2.414 GHz, and within a fixed given bandwidth, two mutually orthogonal OAM modes at a distance of 442 m (3536λ) from the phase-detecting interferometer. After having verified that the phase properties of the twisted beam were preserved, by analysing the beam shape with an intensity/spectrum analyser, we transmitted the two OAM modes from the lighthouse of San Giorgio Island in the direction of the balcony of Palazzo Ducale in Venice (Italy), where they were received. The HPBW diameter of the parabolic antenna at that distance was 67 m. During the experiment, we measured a maximum signal power $P_{max} = 30.7$ dBm, with a background noise of -87 dBm generated by external radio sources. The noise background that we characterized with the help of a digital spectrum analyser was dominantly caused by external sources (see table A.4 in the appendix).

At the phase singularity point we expected the intensity to drop almost to zero, as found in experiments at optical frequencies. The narrow zone where the central singularity was located, defined by a 10 dB (i.e. tenfold) drop in the mean field intensity, had a diameter of about 2λ. This small region was contained inside a wider zone with a diameter of $\sim$190 cm ($\sim$15λ) where a 3–5 dB drop in the mean field intensity was observed. Outside this region, at distances larger than 2 m ($\sim$16λ) from the singularity, the field intensity was found to be more stable and flatter. The measured signal intensity was only 3 dB lower than expected from a non-helicoidal parabolic antenna with the same diameter and focal length.

Due to propagation effects, the signal intensity near the singularity, where the electric field tends to zero, exhibited a more uniform and flatter intensity profile than expected from a coherent beam with a Laguerre–Gaussian profile. The phase distribution of the entire antenna lobe was preserved. This actually resembles the behaviour of incoherent beams carrying OAM. Such beams preserve the phase profile but the region of the lobe in which the singularity is located appears much more filled by the signal because of the large width of the transmission band and, in our case, probably also because of the shape of the transmitting antenna. The only insignificant variable interference effects noted during the experiments were due to reflections of the beam from the water surface of the lagoon that varied with the tidal height of the sea.

By using an interferometric phase discrimination method we were able to separate the two OAM modes by identifying their 'phase fingerprints' [10, 11, 21, 23, 24]. The receiving station consisted of a commercial off the shelf (COTS) frequency-modulation (FM) radio module receiver fed by two identical 16.5 dBi Yagi–Uda antennae (hereafter called antenna A and antenna B) connected together with 180°-phase-shifted cables through a beam adder module, in order to obtain a phase-difference interferometer. We decided to use such directive antennae to spatially reduce any possible background interference due to the presence of other WiFi sources. The antenna parameters are given in the appendix. Antenna A was mounted on a mechanical translator oriented towards the direction of the transmitting station to select one of the two channels by exploiting the spatial phase front properties of different OAM states present in the two beams, whereas antenna B could be moved mechanically in the orthogonal horizontal direction only.

The interferometer measured the phase difference between the two antennae, A and B, and therefore characterized the spatial phase properties of the beams that are the fingerprints of the vorticity OAM states of the field. To discriminate between the two different spatial modes of the EM field, we aligned antenna A, antenna B and the field singularity along a line parallel

to the horizon, and the singularity was positioned in the middle of the segment delimited by antennae A and B (see the scheme in the appendix, figure A.6). If the setup were perfectly aligned, the twisted EM wave with $\ell = 1$ would have produced an exact 180° azimuthal phase difference between the two antennae, subsequently compensated for by the cable electric delay, thus producing an intensity maximum. The untwisted beam, with 0° azimuthal phase difference, would have produced an intensity minimum for the same settings.

EM waves with wavelength λ, propagating along the two paths from the source to the two receiving antennae A and B, acquired a total phase difference ϕ that depends on the angle θ between the incident plane wavefront and the interferometer baseline, the relative azimuthal term between the two receiving antenna ϕ_ℓ due to the beam vorticity ($\phi_\ell = 0$ when $\ell = 0$ and $\phi_\ell = \pi$ when $\ell = 1$) and a generic additional spatial/temporal phase term ϕ_0 introduced by the experimental setup (e.g. cable delay, imperfect parallelism of the receiving antennae, etc). This total phase difference can be approximated by

$$\phi = 2\pi \frac{d \sin \theta}{\lambda} + \phi_\ell + \phi_0,$$

where d is the separation of the two antennae. The signal was collected equally by antennae A and B in phase and the signal of antenna A arrived at the signal adder 180° out of phase with respect to that of antenna B because of the electric $\lambda/2$ cable delay, resulting in a difference signal configuration, $|A - B|$, such that

$$|V_A - V_B| \approx \left| V_0 - V_0 \mathrm{e}^{\mathrm{i}\phi} \right| = 2V_0 \sin \frac{\phi}{2},$$

where V_0 is the voltage measured at the antenna cable end (receiver input). The bearing to the transmitter is, in the ideal case, determined by a minimum or total absence of signal. A maximum is obtained when $\phi = (k+1)\pi$ and k is an integer.

By adding a phase delay to the signal from antenna A, one can change the pointing direction of the antenna system in such a way that the segment $A - B$, delimited by the two antennae, would effectively rotate rigidly around the field singularity in the direction orthogonal to the propagation of the EM signal, with the result of moving the position of the null interference fringes and compensating for the presence of additional phases and the inclination of the interferometric base with respect to the direction of the source. Alternatively, a similar compensation is obtained by moving antenna A along the direction of the source by a quantity $\Delta x = \lambda n / 2\pi$. Consequently, the phase difference between the two paths can be written as

$$\phi = 2\pi \frac{d \sin \theta}{\lambda} - n.$$

The parameter n can be adjusted to improve the tuning of the receiving system and read a signal minimum in the exact direction to the transmitting antenna. Here, n is negative when antenna A is moved towards the source.

If the beam carries OAM, the phase distribution of the wavefront arriving at antennae A and B will exhibit a characteristic topological signature. In the simplest case, when the centre of the vortex coincides with the centre of the interferometer, the two antennae will experience a phase gap due to the OAM of the EM wave $\phi_\ell = \ell\pi$ and a maximum of the signal is obtained when the phase factor is

$$\phi = 2\pi \frac{d \sin \theta}{\lambda} - n + \ell\pi = (k+1)\pi, \quad k \in \mathbb{Z},$$

where $\mathbb{Z}$ is the set of all integer numbers. When $\ell = 1$, a maximum for the vortex is achieved when $n = 0$ and $k = 0$. Because of destructive interference the $\ell = 0$ signal intensity will at the same time experience a minimum. On the other hand, a maximum for the $\ell = 0$ mode will be obtained when $n = -\lambda/2$, corresponding to a minimum for the vortex. Following these considerations, we aligned the interferometer so as to have the field singularity at the midpoint of the line joining the two receiving antennae (i.e. the interferometer baseline) and obtained a phase gap $\phi_\ell = \pi$ between the two antennae expected during the reception of the $\ell = 1$ vortex. To better optimize the interference fringe structure we oriented the baseline by an inclination $\theta \sim 10°$ with respect to the balcony in order to be orthogonal to the incoming beam. During the experiment, the main practical difficulty was that of positioning the singularity at the midpoint between the two Yagi–Uda antennae: this problem was solved with the find-and-track direction method, also known as the 'fox-hunting' method [25], commonly used to locate a radio transmitter with high precision.

In order to have a simple, straightforward and practical method to discriminate between the two orthogonal OAM channels, transmitted on the same carrier frequency, we frequency modulated them with constant-level audio signals at different modulation frequencies (400 and 1000 Hz for the untwisted and twisted waves, respectively) by injecting a -5 dBm monophonic audio signal into the video band of each transmitter. The thus-modulated radio signals were received by the two Yagi–Uda antennae, summed by a 3 dB power splitter/combiner (Mini-Circuits ZX10-2-42+) and then demodulated in the FM receiver into monophonic audio signals that were subsequently digitally sampled, recorded and analysed in real time with 32-bit resolution. Each dataset so produced was 22 870 008 bytes long.

The total signal loss measured in the receiving line of the interferometer was 6 dB. In order to reduce the power of the signal we inserted a calibrated 10 dB attenuator into the receiving line, so that the audio digitizer connected to the receiver output would not saturate due to overvoltage. In a conventional single-antenna receiver setup that detects linear momentum only, the two radio signals were audible simultaneously. By mechanically moving the antenna A with respect to B to select one of the two orthogonal OAM beams, one signal was alternately suppressed with respect to the other due to the different spatial phase signature of the two OAM states. We adjusted the baseline in order to optimize the discrimination of the two different OAM channels by moving antenna A.

Since an FM transmission has the property of generating a constant amplitude output, we adjusted the output of the two transmitters to measure the same receiver output voltage, 1 volt in continuous current (VCC) for each channel. In this way, we were able to characterize the transition between equal-intensity twisted and untwisted channels. Figure 2 shows the maximum positive voltage of the signal measured at the output of the antenna receiver and amplifier. The untwisted beam (line marked 'o') showed destructive interference in the interval 8.5–9.4 cm (approximately 0.7λ–0.8λ) from the initial antenna position. In the corresponding audio track, the carrier disappears and the 400 Hz tone is suddenly replaced by white noise, which appears louder due to the automatic gain control (AGC) of the receiver. This is a clear indication of destructive interference. Similar behaviour was observed in two other smaller regions and is possibly due to the effects of the secondary Yagi lobes that were not considered in our autocorrelation analysis. The twisted beam (red continuous line), on the other hand, presented a richer forest of alternating maxima and minima; only near the initial position of the antenna (0.4–1.6 cm) was a wide region of total destructive interference observed.
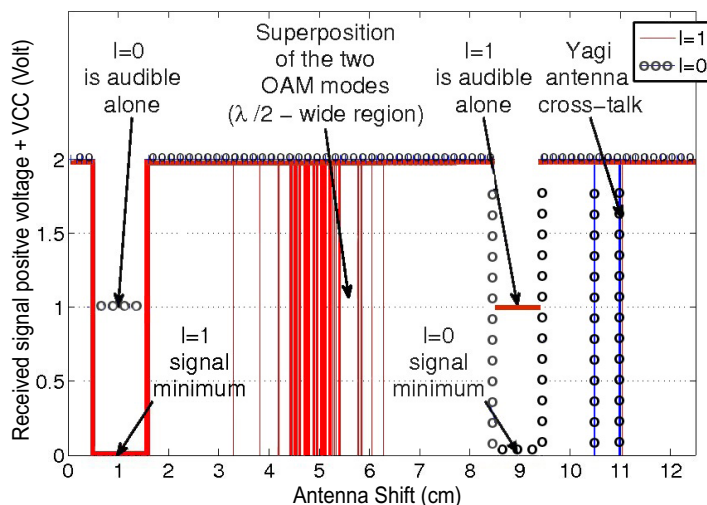
Figure 2. Diagram of the monophonic audio recordings of the twisted/untwisted beams. The output of the two transmitters was adjusted to ensure the same maximum input voltage of 2 V when both channels were present, and 1 VCC max for each individual channel. The first minimum is found at about 1 cm of antenna shift for the $\ell = 1$ mode (continuous line). Here the $\ell = 0$ channel (marked with the symbol 'o') has a maximum and the associated audio tone is clearly audible. The same was found for the $\ell = 0$ mode around the 9 cm antenna position. The inner boundaries of the two minima regions are separated in distance by half the radio wavelength. Between these positions there was a forest of minima of the $\ell = 1$ mode, a phenomenon due to the sampling of the field from a finite-sized antenna. Beyond the minimum located at 9 cm, two additional alternating signal minima due to the cross-talk of the two Yagi–Uda antennae were found.

In figure 3, we display the audio frequency spectrum, from 0 to 3 kHz, of the two separate OAM channels ($\ell = 0$, upper panel; $\ell = 1$, middle panel) obtained from the best acquisition made during our OAM tuning experiments. Each single channel is said to be tuned when the other one experiences destructive interference and the corresponding audio tone disappears. In the lower panel, we show the spectrum of the superposed $\ell = 0$ and $\ell = 1$ channels, measured outside the regions of destructive interference. This result is confirmed by the Tolonen–Karjalainen autocorrelation for multi-pitch detection [26], as shown in figure 4. Whereas the $\ell = 0$ mode always showed a clear autocorrelation, the $\ell = 1$ mode always presents a series of harmonic tones at higher frequencies.

An audio recording, split into three MP3 files of the tuning between the two OAM channels, is provided as additional material, available at stacks.iop.org/NJP/14/033001/mmedia. The first audio file (movie 1) is the recording of the spatial tuning of the channel without OAM only. One can hear the main tone at 400 Hz and then strong white noise at the position where antenna A, moving in the direction of the source with respect to antenna B, reaches the point where the signal is cancelled by the interferometer. The second file (movie 2) shows that the twisted beam has a much richer spatial structure than that of the untwisted beam. Finally, the third file (movie 3) is the recording of the vortex tuning between the two different OAM states transmitted simultaneously on the same frequency and used in the data analysis reported in figures 2–4.
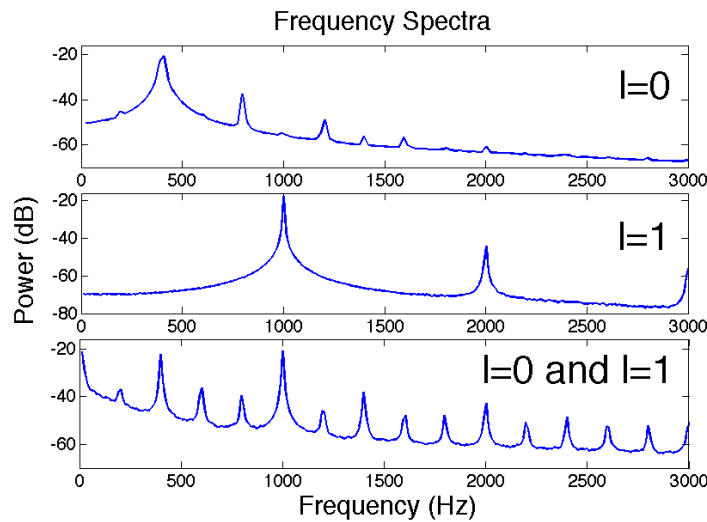
Figure 3. Spectral analysis of the demodulated audio signal when the antenna interferometer was tuned by the spatial motion of one antenna to receive two independent and superposed OAM modes in the same frequency band. The spectra are truncated at 3 kHz for better clarity. Upper panel: audio frequency spectrum of the beam in the region where the interferometer is tuned for the $\ell = 0$ mode signal. Clearly visible is the main peak at 400 Hz followed by the higher-frequency harmonics. The power of the signal is distributed with decreasing power at higher frequencies. Middle panel: audio spectrum in the position where only the $\ell = 1$ mode audio signal is audible. Also in this case the power is distributed with less power for higher-frequency harmonics of the 1 kHz main frequency. In both the two spectra there are no spurious frequencies introduced by the other twisted signal. Lower panel: audio spectrum of the signal where the two twisted beams are not separated. Both the audio frequencies are visible.

Already with this setup, one can obtain four physically distinct channels on the same frequency by additionally introducing the use of polarization (SAM), which is independent of OAM. A further five-fold multiplicative factor from implementing multiplexing would yield a total of 20 channels on the same frequency. The utilization of multiport techniques (e.g. MIMO) could increase the capacity further.

5. Conclusions

Our experimental findings that EM OAM can be used for increasing radio transmission capacity without increasing bandwidth is likely to open up new perspectives on wireless communications and radio-based science. History tells us that Marconi invented the wireless telegraph and from that the communication world spread its branches in all directions [1]. All current radio communication services are based on various forms of phase, frequency and/or amplitude modulation of the EM radiation in the form of EM linear momentum (i.e. integrated Poynting vector or energy flux). In order that many different broadcasting stations are able to transmit simultaneously without overlapping their radio signals, Marconi suggested
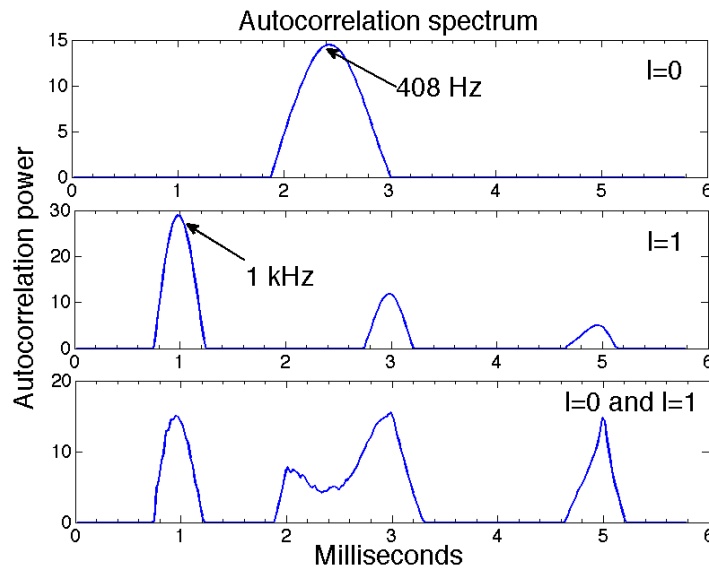
Figure 4. Autocorrelation spectral analysis of the audio transmission in three different antenna positions. Upper panel: the $\ell = 0$ mode ($\sim$408 Hz) detectable when the antenna is at a position between 0.4 and 1.6 cm. Middle panel: the $\ell = 1$ (1 kHz), from 8.5 to 9.4 cm, with the exception of the two small intervals where a cross-talk of the two antennae was observed. In the lower panel, the superposition of both the audio signals at 400 and 1 kHz is clearly evident, showing the impossibility of separating the two channels when the moving antenna is in the interval (1.8–8) cm.

that the total available spectrum of radio frequencies be divided into many non-overlapping frequency subbands [23]. Now, the wide use of wireless communication has unavoidably led to the saturation of all available frequency bands, even after the adoption of artificial techniques that increase band capacity. We have experimentally shown that by using helicoidal parabolic antennae, the use of OAM states might dramatically increase the capacity of any frequency band, allowing the use of dense coding techniques in each of these new vortex radio channels. This might represent a concrete proposal for a possible solution to the band saturation problem.

Moreover, our experimental findings demonstrate that the spatial phase signature was preserved even in the far-field region and for incoherent non-monochromatic wave beams. These results open up new perspectives not only for wireless communication but also for physics and astronomy, including the possible detection of Kerr black holes in the test general relativity [21].

Acknowledgments
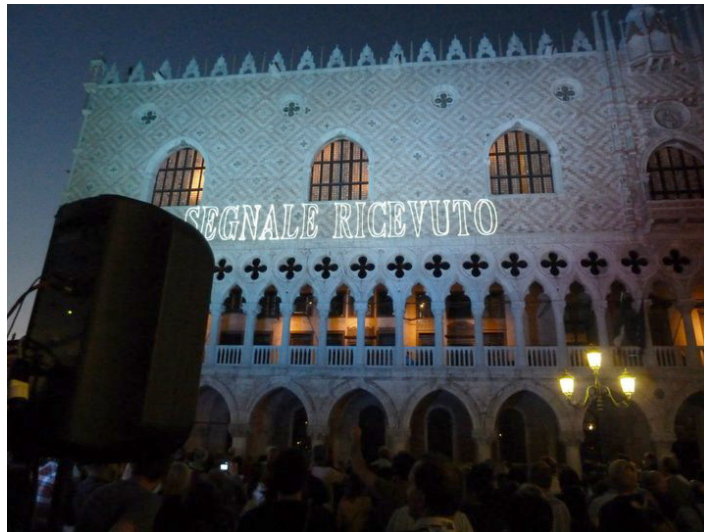
Figure A.1. Public announcement of the reception and tuning of the twisted signal 'segnale ricevuto' (signal received).

Appendix

A.1. Waves on waves

'Onde sulle Onde', a public experiment. The final results of this experiment were publicly demonstrated on 24 June 2011 on Piazza San Marco, Venice, in the presence of the international press, experts, well-known personalities and the general public. In the style of Guglielmo Marconi, we realized this first public demonstration of radio vortices by also involving ordinary people in the experiment—a different way to communicate science. A light and sound show with projections onto the façade of Palazzo Ducale explained to the audience what the experimenters were doing. More than 2000 people attended the 'live' experiment at 21:30 local time and when the signal was tuned from vorticity zero to vorticity one at the same frequency and transmitting simultaneously, a rifle shot was heard, in honour of the first radio transmission made by Guglielmo Marconi in 1895. After this, on the façade of Palazzo Ducale the words 'segnale ricevuto', which in Italian means 'signal received', were projected. Several video recordings of this event, made by spectators and radio amateurs, can be found on YouTube on the Internet (figure A.1).

A.2. Hardware

To demonstrate the feasibility of implementing multiple radio communication channels on the same frequency, discriminated only by their OAM, we adopted a very basic hardware

Figure A.2. One of the Yagi–Uda antennae of the interferometer mounted on the top of an isolated plastic pillar.
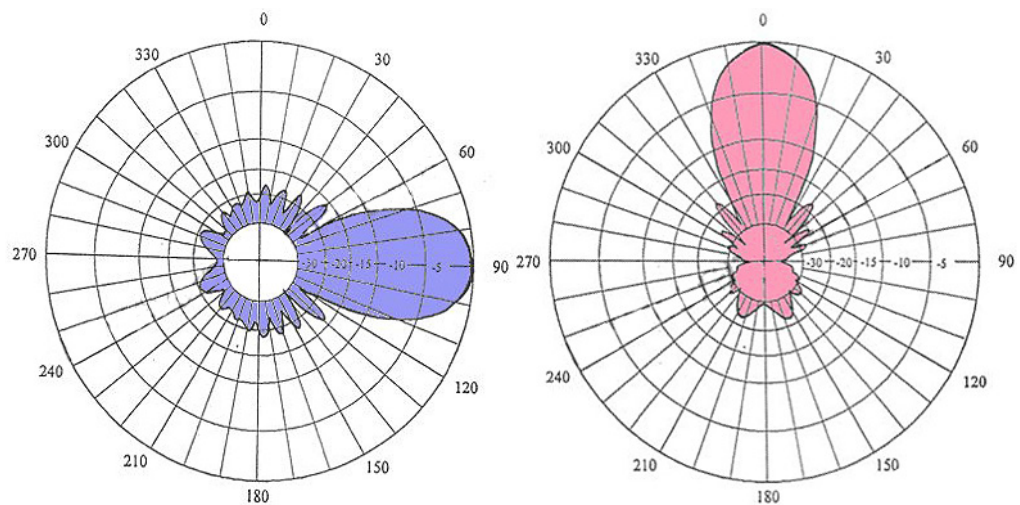
Figure A.3. Horizontal and vertical linear momentum radiation (Poynting vector) diagrams of the lobes of the COTS Yagi–Uda antennae used in the interferometer. The diagrams show the usual complicated pattern of the secondary lobes.

configuration, comprising a couple of commercial audio/video tuneable receivers and 2 W transmitter modules feeding the twisted parabolic antenna for the twisted beam with OAM ($\ell = 1$), and a 16.5 dBi Yagi–Uda antenna for beams without OAM ($\ell = 0$) (figures A.2 and A.3).

The COTS receiver was connected to two identical 12-element, 16.5 dBi gain Yagi–Uda antennae, tuned to 2.4 GHz and mounted on the top of two identical plastic columns ($\varepsilon \approx \varepsilon_0$). The baseline between the receiving antennae was 4.50 m, with laser-controlled levelling and calibrated mutual distance. Each of the receiving antennae was mounted on a mechanical

Table A.1. Main characteristics of the Yagi–Uda antennae used in the experiment.

Operating frequency (MHz)	2400–2480
Average gain	16.5 dBi
Size	$45 \times 5 \times 4$ cm
Vertical/horizontal irradiation	$35°$
Impedance	$50\,\Omega$
SWR (standing wave ratio)	<1.3

Table A.2. Azimuthal elevation required to obtain the shape of the helicoidal parabolic antenna from the initial parabolic pattern expressed in wavelength units and centimetres.

Azimuthal angle	Elevation (in units of λ)	Elevation (cm)
$0 = 2\pi$	1/2	6.25
$\pi/2$	3/4	4.69
π	1/4	3.12
$(3/2)\pi$	1/8	1.56

**Figure A.4.** The helicoidal parabolic antenna.

translator that provided fine-tuning in an interval of 10 cm ($\sim 0.8\lambda$). The cable connections were made with a Belden H155 Wifi coaxial cable, $50\,\Omega$ impedance and 5.4 mm diameter. The velocity factor in the cable for this type of cable is 79% with 9.3 dB loss $(100\,\text{m})^{-1}$, characterized by the producer at a frequency of 100 MHz. Then, the half-wavelength cable junction used to build the phase difference interferometer resulted to be 4.94 cm long (table A.1).

Table A.3. Main characteristics of a non-helicoidal parabolic antenna lobe width having the same diameter and focal ratio as the twisted parabolic antenna. The theoretical gain is expressed as a function of the angular deviation from the beam direction.

dB contour down (degrees)	0	0.25	0.5	1	24	26
Full beamwidth (degrees)	0	3.13	4.42	6.25	8.84	10.83
Gain dBi	24.2	23.95	23.7	23.2	22.2	21.2
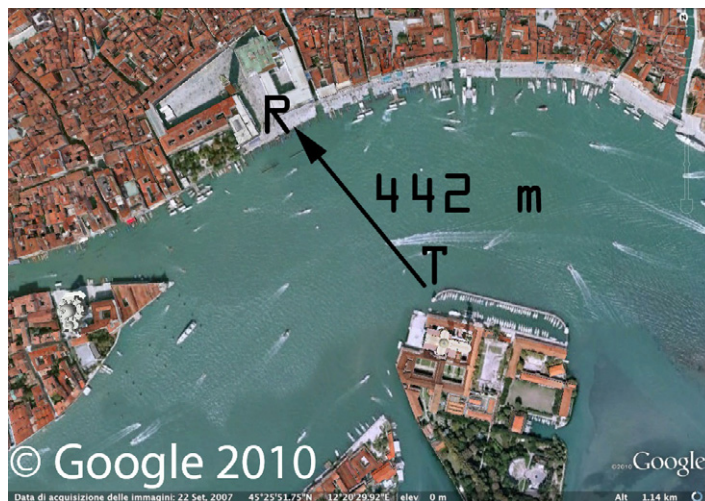
Figure A.5. View of the San Marco experiment site in Venice, Italy. Reproduced from Google Earth. © 2012 Google.
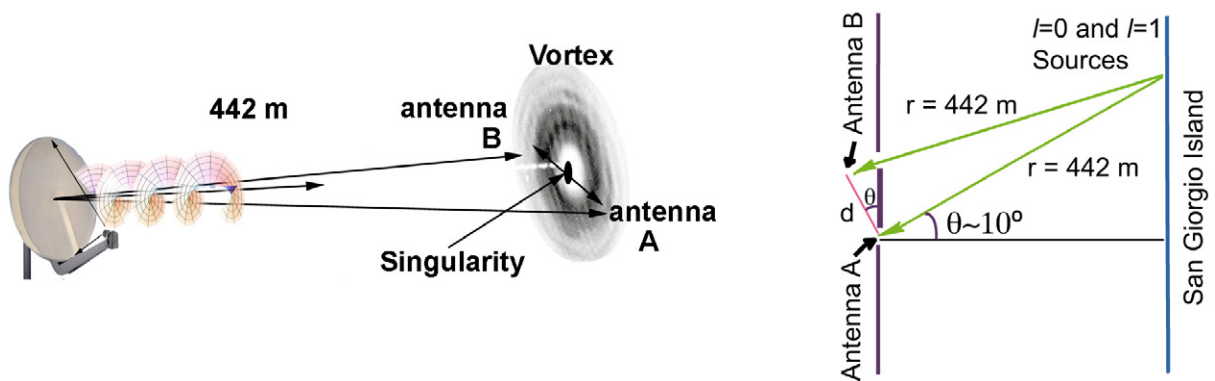
Figure A.6. Sketch of the experiment in San Marco (not to scale). From left to right: the transmitting antenna, the twisted radio beam and the two antennae *A* and *B* aligned with the singularity of the beam. The two receiving antennae were positioned so that the singularity was located on the baseline between the two antennae at the midpoint of the segment *AB*. Rightmost panel: schematic representation of the experiment.

Figure A.7. Lobby of Palazzo Ducale, 50 m long: location of the receiving station.

Table A.4. The electrosmog background measured in the lobby of Palazzo Ducale (vertical and horizontal linear polarizations).

Loggia 1	Max (dBm)	Avg (dBm)
2.414 GHz Vpol	−87.5	−88
2.414 GHz Hpol	−89	−89
Loggia 13	**Max (dBm)**	**Avg (dBm)**
2.414 GHz Vpol	−87.9	−89
2.414 GHz Hpol	−88	−89
Loggia 25	**Max (dBm)**	**Avg (dBm)**
2.414 GHz Vpol	−86	−87
2.414 GHz Hpol	−88	−88

A.3. Transmitter/receiver modules

The audio and radio signals used in the calibration and with the actual radio transmission were generated with commercial high-quality super-heterodyne FM transmitting modules. The output impedance was 75 Ω. The deviation in frequency relative to the carrier frequency (2.414 GHz) due to the FM modulation (15 MHz) can be considered negligible and not to cause significant distortion of the vortex or a consequent change of the topological charge generated by the twisted parabolic antenna.

A.4. Offset helicoidal parabolic antenna

From a pair of identical, 15° offset, 80 cm diameter steel parabolic antennae, the dish was transformed into a vortex reflector by elevating, from the original shape, the surface of the quantities reported in the table for given values of the azimuthal angle. (see figures A.4 and tables A.2 and A.3).

A.4.1. Site of the San Marco experiment. Transmitter (T): Torretta della Compagnia della Vela in San Giorgio (lighthouse). Altitude, 10 m msl (mean sea level); lat, 45°25′48″ N, long, 12°20′35″ E. Receiving station (R): Loggetta del Palazzo Ducale. Altitude, 16 m msl; lat, 45°26′00″ N; long, 12°20′25″ E. Geometrical distance 442 m as measured with GPS and Google Map (figures A.5 and A.6).

A.4.2. Electrosmog–Loggia (Lobby) of Palazzo Ducale. Date: 13 June 2011, Time: 9.00-9.45 GMT The height of the balcony rail is 130 cm, and the distance between two columns of the lobby is 214 cm (see figure A.7 and table A.4).

References

[1] Dunlap O E Jr 1937 *Marconi: The Man and His Wireless* (New York: Macmillan)
[2] Li G and Stüber G L (ed) 2006 *Orthogonal Frequency Division Multiplexing for Wireless Communications* (New York: Springer)
[3] Thidé B 2011 *Electromagnetic Field Theory* 2nd edn (Mineola, NY: Dover) http://www.plasma.uu.se/
[4] Berestetskii V B, Lifshitz E M and Pitaevskii L P 1982 *Quantum Electrodynamics* vol 4, 2nd edn (Oxford: Butterworth-Heinemann)
[5] Mair A, Vaziri A, Weihs G and Zeilinger A 2001 Entanglement of the orbital angular momentum states of photons *Nature* **412** 313–6
[6] Leach J, Padgett M J, Barnett S M, Franke-Arnold S and Courtial J 2002 Measuring the orbital angular momentum of a single photon *Phys. Rev. Lett.* **88** 257901
[7] Tamburini F and Vicino D 2008 Photon wave function: a covariant formulation and equivalence with QED *Phys. Rev.* A **78** 052116
[8] Molina-Terriza G., Torres J P and Torner L 2007 Twisted photons *Nature Phys.* **3** 305–10
[9] Gibson G, Courtial J, Padgett M J, Vasnetsov M, Pas'ko V, Barnett S M and Franke-Arnold S 2004 Free-space information transfer using light beams carrying orbital angular momentum *Opt. Express* **12** 5448–56
[10] Tamburini F, Mari E, Thidé B, Barbieri C and Romanato F 2011 Experimental verification of photon angular momentum and vorticity with radio techniques *Appl. Phys. Lett.* **99** 204102
[11] Palacios D M, Maleev I D, Marathay A S and Swartzlander G A Jr 2004 Spatial correlation singularity of a vortex field *Phys. Rev. Lett.* **92** 143905
[12] Grier D G 2003 A revolution in optical manipulation *Nature* **424** 810–6
[13] Vaziri A, Weihs G and Zeilinger A 2002 Superpositions of the orbital angular momentum for applications in quantum experiments *J. Opt. B: Quantum Semiclass. Opt.* **4** S47–51
[14] Anzolin G, Tamburini F, Bianchini A, Umbriaco G and Barbieri C 2008 Optical vortices with star light *Astron. Astrophys.* **488** 1159–65
[15] Thidé B *et al* 2007 Utilization of photon orbital angular momentum in the low-frequency radio domain *Phys. Rev. Lett.* **99** 087701
[16] Elias II N M 2008 Photon orbital angular momentum in astronomy *Astron. Astrophys.* **492** 883–922
[17] Harwit M 2003 Photon orbital angular momentum in astrophysics *Astrophys. J.* **597** 1266–70
[18] Berkhout G and Beijersbergen M 2008 Method for probing the orbital angular momentum of optical vortices in electromagnetic waves from astronomical objects *Phys. Rev. Lett.* **101** 100801
[19] Tamburini F, Anzolin G, Bianchini A and Barbieri C 2006 Overcoming the Rayleigh criterion limit with optical vortices *Phys. Rev. Lett.* **97** 163903
[20] Lee J H, Foo G, Johnson E G and Swartzlander G A Jr 2006 Experimental verification of an optical vortex coronagraph *Phys. Rev. Lett.* **97** 053901
[21] Tamburini F, Thidé B, Molina-Terriza G and Anzolin G 2011 Twisting of light around rotating black holes *Nature Phys.* **7** 195–7

[22] Uda S 1927 High angle radiation of short electric waves *Proc. IRE* **15** 377–385
     Yagi H 1928 Beam transmission of ultra-shortwaves *Proc. IRE* **16** 715–40
     Uda S 1930 Radiotelegraphy and radiotelephony on half-meter waves *Proc. IRE* **18** 1047–63
[23] Marconi G 1941 *Scritti di Guglielmo Marconi* (Rome: Reale Accademia d'Italia) http://www.liberliber.it/
     biblioteca/m/marconi/scritti/pdf/marconi_scritti.pdf
[24] Torner L, Torres J and Carrasco S 2005 Digital spiral imaging *Opt. Express* **13** 873–81
[25] Chang K 2000 *RF and Microwave Wireless Systems* (New York: Wiley)
[26] Tolonen T and Karjalainen M 2000 A computationally efficient multipitch analysis model *IEEE Trans. Speech
     Audio Process.* **8** 708–16